Angewandte Chemie
Eine Zeitschrift der Gesellschaft Deutscher Chemiker

Supporting Information

© Wiley-VCH 2006

69451 Weinheim, Germany

Mechanical and Dielectric Properties of Pure-Silica-Zeolite Low-*k* Materials

Zijian Li[1], Mark C. Johnson[2], Minwei Sun[1], E. Todd Ryan[3], David J. Earl[4], Wolfgang Maichen[5], Jeremy I. Martin[3], Shuang Li[1], Christopher M. Lew[1], Junlan Wang[2], Michael W. Deem[4], Mark E. Davis[6], and Yushan Yan[1]*

[1] Department of Chemical and Environmental Engineering, University of California, Riverside, California 92521, USA.

[2] Department of Mechanical Engineering, University of California, Riverside, California 92521, USA.

[3] Advanced Micro Devices Inc., Hopewell Junction, New York 12533, USA.

[4] Department of Bioengineering, Physics and Astronomy, Rice University, Houston, Texas 77251, USA.

[5] Teradyne Inc., Agoura Hills, California 91301, USA.

[6] Chemical Engineering, California Institute of Technology, Pasadena, California 91125, USA.

Materials and Methods

Synthesis of PSZ MFI seeded growth film

PSZ MFI seeded growth films were synthesized hydrothermally following a published procedure [1]. The precursor was prepared by adding 2.69 g of TPAOH (tetrapropylammonium hydroxide, 40wt%, SACHEM) with 98.93 g of double deionized (DDI) water under stirring for 10 minutes. Next, 5 g of TEOS (tetraethylorthosilicate, 98wt%, Aldrich) was added dropwise. A clear solution with a molar ratio $40SiO_2$: 9TPAOH: $9500H_2O$: 160EtOH was then obtained.

A piece of silicon wafer (~2.5×2.5 cm) was immersed in an aqueous suspension of silicalite seeds crystals of ~80 nm for 2 minutes and then dried in ambient air. Seeds were synthesized by the procedure from ref. [2]. This procedure was repeated three times.

Then the silicon wafer was then placed vertically into a Teflon® holder, which was subsequently placed into a Teflon®-lined autoclave. Crystallization was carried out at 413 K for 48 hours. The samples were washed with DDI water and blow-dried in a nitrogen stream.

PSZ MFI seeded growth films were polished by a Buehler polisher to obtain a smooth surface. Then the films were heated at a rate of 1K/min to 773 K and calcined at 773 K for 8 hours in air before nanoindentation and k measurements.

Synthesis of large zeolite crystals

FER: Large PSZ FER crystals were prepared solvothermally according to a published procedure [3]. Briefly, a mixture of 24.97 g of py (pyridine, 99wt or v%, Aldrich), 4.83 g of ap (1-amino-n-propane, 98%, Aldrich) and 2.88 g of DDI water was stirred for 30 minutes. Then 1.14g of HF/pyridine (HF/py, 70 wt% HF, Aldrich) was added dropwise to the synthesis solution with stirring in cold water bath. After 10 minutes, 1.80g of fumed silica (99.8%, Cabosil-M5, Aldrich) was added to the solution to obtain a clear highly viscous gel. After stirring overnight, the synthesis solution in a molar ratio of $1.5SiO_2$: 2HF/py: 4ap: $8H_2O$: 16py was sealed in Teflon®-lined autoclaves at 453 K for ~14-20 days under autogenous pressure and static conditions.

Solids were recovered and rinsed with ethanol and DDI water twice. Solids were then ultrasonicated for 8 hours in DDI water during which the DDI water was changed every two hours. The crystals were dried for further characterization.

MFI: Large PSZ MFI crystals were synthesized by the method developed by Qiu et al [4]. Briefly, a reaction mixture, containing 0.89 g HF (40 wt%, Aldrich), 7.26 g TPAOH, and 28.17 g DDI water was obtained with a final molar ratio of 1.5HF: TPAOH: 128.6 H_2O. A piece of silicon wafer about 0.4 g was placed into the Teflon®-lined autoclave together with the reaction mixture. The crystallization was carried out at 453 K for 20 days at autogenous pressure and static conditions. A SEM image of PSZ MFI image is shown in Fig. S1A.

CHA: Large B-CHA was synthesized by mixing 1.45 g of SiO_2 (99.8%, Cabosil-M5, Aldrich), 0.12 g of NaCl (Certified ACS, Fisher), 0.12 g of H_3BO_3 (Certified ACS, Aldrich) and 9.7 g of TMAdaOH (N,N,N-trimethyl-1-adamantammonium hydroxide,0.62 mol/l) in a sealed container. After aging overnight the gel was transferred to Teflon®-lined autoclaves. Crystallization was carried out at 433 K for 4 days. The samples were washed with DDI water and dried. A SEM image of B-CHA is shown in Fig. S1C.

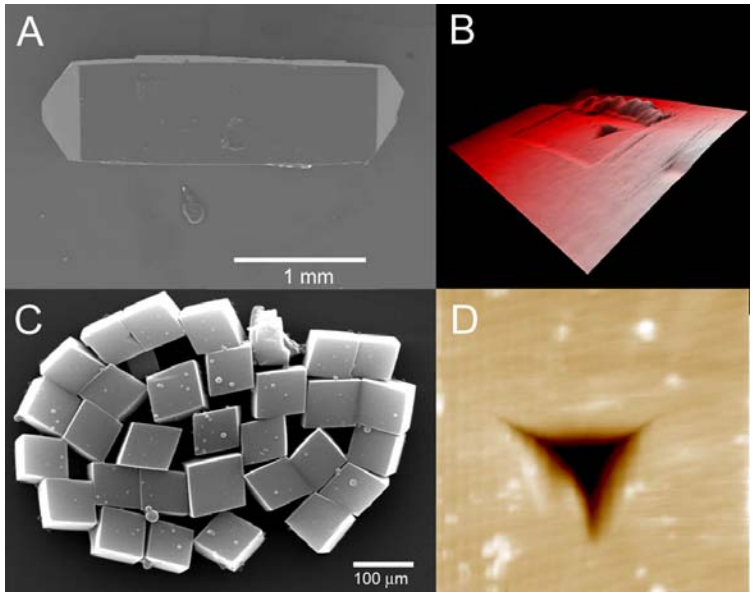

Fig. S1 (A) SEM image of a MFI single crystal with a size of 2.7×0.7x0.7 mm. (B) SPM image of the indents on MFI by the same Berkovich tip; the scan area is 3×3 μm. (C) SEM image of a group of CHA crystals with a size of about 100x100x100 μm. (D) SPM image of the indent on CHA scanned by the same Berkovich tip; the scan area is 3×3 μm.

Nanoindentation

A Ubi1 nanomechanical test instrument (Hysitron) was used to perform nanoindentation experiments and in situ scanning probe microscopy. The resolutions of the force and displacement are 1 nN and 0.04 nm, respectively. A Berkovich tip was used to test the zeolite crystals. The tip has a radius of approximately 150 nm and a total included angle of 142.3 degrees and a half angle (effective cone angle) of 65.35 degrees. A very thin layer of super glue was applied between the crystals and substrate before single indentation. The super glue layer has to be carefully spread so that it would not contaminate the surface of the crystals. Multiple indentations to various depths at different locations on each sample were performed. Load versus displacement curves with indent depth ranging from 16 to 250 nm and with loads from 200 to 12,000 μN showed the reproducibility of E and hardness at different indentation depths.

During an indentation, the force and displacement are monitored and a force versus displacement curve is produced. Following the procedures developed by Vlassak and Nix [5]. The reduced indentation modulus is determined from the force vs. displacement curve using Eq S1:

$$E_r = \frac{\sqrt{\pi}}{2\sqrt{A(h_c)}} S \qquad \text{S(1)}$$

where S is the measured contact stiffness and is defined as the slope at initial unloading of the force-displacement curve, and $A(h_c)$ is the contact area as a function of contact depth h_c. The tip area function, $A(h_c)$, is calibrated prior to experiments by indenting a standard fused quartz sample. The reduced indentation modulus is a parameter which accounts for the deformations both in the material and the diamond indenter tip and is defined as in Eq. S2

$$\frac{1}{E_r} = \frac{1-\nu_i^2}{E_i} + \frac{1}{M_s} \qquad \text{S(2)}$$

where E_r is the reduced indentation modulus, ν_i and E_i are the Poisson's ratio and elastic modulus of the indenter, and M_s is the indentation modulus of the sample which is a parameter accounting for the anisotropic material properties along multiple directions of the material under investigation. In this case, the indenter is diamond with a Poisson's ratio and E of 0.07 and 1140 GPa, respectively. For isotropic materials, such as the spin-on and polycrystalline films, the indentation modulus (M_s) of the sample is equivalent to the plain strain modulus defined by Eq. S3

$$M_s = \frac{E_s}{1-\nu_s^2} \qquad \text{S(3)}$$

where ν_s and E_s are the Poisson's ratio and Young's modulus of the sample, respectively. Once the reduced indentation modulus (i.e., E_r) is obtained from the indentation load vs. displacement data, the Young's modulus E of the sample is calculated using Eq. S2 and S3 assuming a Poisson's ratio of 0.25.

The hardness of the zeolite films is derived from the unloading portion of the load-displacement curve of an indent following the procedures of Oliver and Pharr [6]. Hardness is defined as the maximum load P_{max} divided by the area of contact in Eq. S4,

$$H = \frac{P_{\max}}{A(h_c)} \qquad \text{S(4)}$$

where $A(h_c)$ is the contact area as a function of contact depth h_c.

Fig. S1A, 1B, 1C, and 1D show the SEM images of the MFI and CHA single crystals and the scanning probe microscope (SPM) images of the indents, scanned by the indenter on MFI and CHA crystals.

Nanoindention was only conducted on non-calcined FER, CHA and MFI single crystals because efforts to prepare large single crystals without template by calcinations were unsuccessful due to easy cracking of crystals at this size. However, it was found that the E and hardness for non-calcined PSZ MFI seeded growth films were nearly identical to the calcined ones. Thus it is reasonable to extend the measured values to those frameworks without organic templates.

Experimental studies on the mechanical properties of zeolite single crystals have been limited. In an early study, PSZ MFI single crystals (~300 μm) were investigated with an in-house-built micromechanical tester. The E was measured to be surprisingly low (~4 GPa) [7]. This is probably due to the fact that the results were obtained by compressing the entire crystal in the tester, and thus defects, which are often present within large crystals, may have adversely affected their measured E value. More recently, E and hardness of PSZ FER single crystals (~200 μm) were evaluated by nanoindentation. An E of 10 GPa and a hardness of 1 GPa were reported [8]. Again, these values are noticeably lower than the values we obtained. It is unclear to us why such low values were obtained in this study.

Measurement of *k* on PSZ MFI seeded growth film

The k value of the MFI seeded growth films was calculated by measuring the capacitance in a metal-insulator-metal configuration fabricated by depositing aluminum dots using thermal evaporation as described in ref. [9]. The thickness of the films was measured by SEM cross-sectional images.

Measurement of *k* on large PSZ FER crystal by Time Domain Reflectometry (TDR)

A Time Domain Reflectometry (TDR) technique was employed to measure the capacitance of FER crystals [10]. The measurement procedure consists of sending a fast step signal into the line under test and recording the reflected signal versus time. The size of a capacitance connected to the open end of the path can be determined by comparing it to a reference measurement without the capacitance [11, 12]. In this case the capacitance C is proportional to the integrated difference (i.e., the area) between the curves with ($V_{sample}(t)$) and without the sample present ($V_{reference}(t)$) as in Eq. S5:

$$C = \frac{1}{2 \times Z_0 \times V_{inc}} \times \int_0^{\infty} \left[V_{reference}(t) - V_{sample}(t) \right] dt \qquad \text{S(5)}$$

where Z_0 is the source (and transmission line) impedance, typically 50 Ω. V_{inc} is the incident step height (in our case the results were already displayed normalized as reflection coefficient, equivalent to setting $V_{inc} = 1$). In reality, the integration does not need to go all the way to infinity because the capacitance is quickly charged up, so the capacitor draws no further current and the two curves converge soon after the transition. The advantage of this method is that it is completely insensitive to signal rise time, signal edge shape, and even series inductance and series resistance between the end of the line and the capacitor. The shape of the reflection signal will change depending on those parameters--series resistance slows the settling down and series inductance introduces ringing. But the difference integral between sample and reference measurement remains constant. This is essential to neglect most effects of the fixture, namely the inductance and resistance of the thin wire we had to use to connect the sample to the end of the transmission line (the fringe capacitance of the wire however adds to the total capacitance and induces a small error).

Fig. S2 shows the schematic experimental setup. A benchtop TDR instrument (Tektronix TDS8000B with 80E04 sampling head) supplies the TDR step signal into a coaxial cable with a SMA launch adapter end, where a FER crystal was mounted. Gold was sputtered on both sides of the crystals. Total system rise time is approximately $T_{10/90}$ = 30 ps, and the impedance is Z_0 = 50Ω. Using conducting silver paste and thin silver-plated wire the sample was attached to the center conductor on one side and to the shield conductor on the other. The reference structure is identical except that the sample and the thin wire are missing. Fig. S3 shows the reflection signals collected for the reference and the sample.

The dielectric constants are calculated by Eq. S6.

$$k = \frac{C}{C_0} \qquad \text{S(6)}$$

where C is capacitance which can be obtained from Time Domain Reflectometry (e.g., Eq. S2). As shown in Fig. S4, thickness, d, is not constant along the plate and thus C_0 is obtained by integration with Eq. S7.

$$C_0 = \iint_{area} \frac{\varepsilon}{l(x,y)} dA = \int_x \int_y \frac{\varepsilon}{l(x,y)} dxdy \qquad \text{S(7)}$$

We also used the setup to measure the *k* values on quartz crystal (1.8mmx3.6mmx41μm, Hoffman Materials Inc.) to calibrate the set up to the known *k* value of 4.58 at 1 MHz [13]. The *k* value measured for FER single crystal is 2.18. It is expected that the *k* value for FER framework without organic structure directing agent should be lower than 2.18.

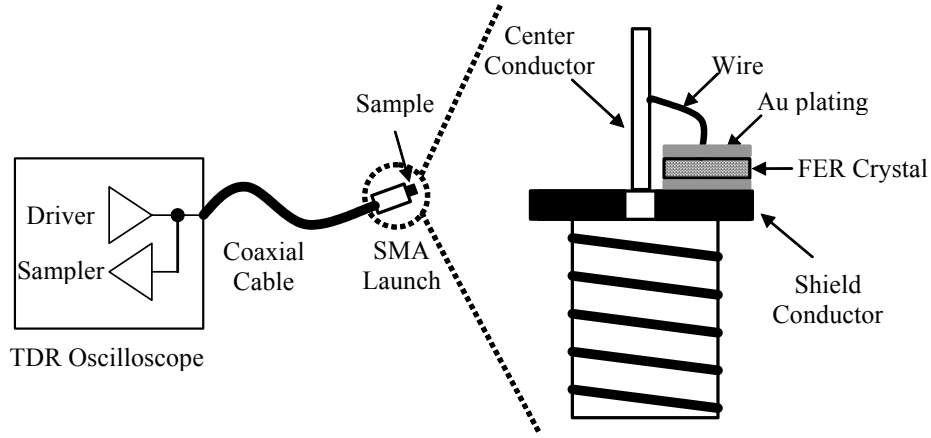

Fig. S2. Experimental setup: block diagram (left), enlarged view of the SMA launch with the mounted sample (right).

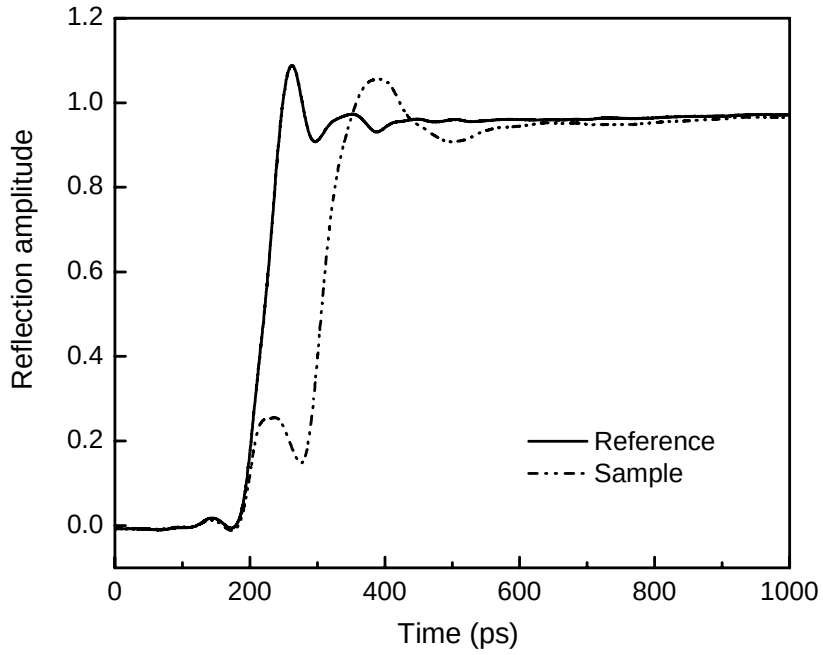

Fig. S3. FER crystal TDR reflection signals for the reference (the solid line) and the sample (the dotted line) respectively.

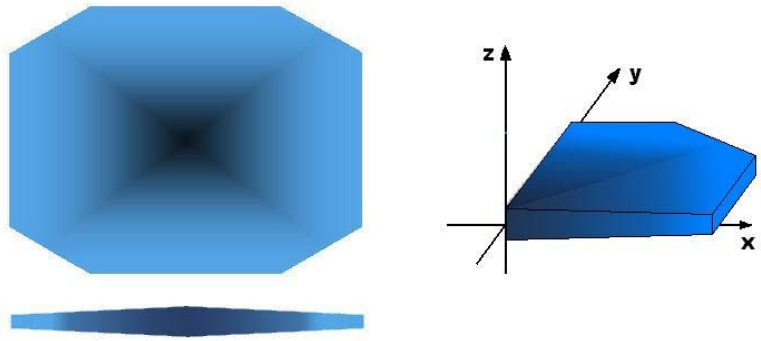

Fig. S4. The schematic of top-view (left top), cross-sectional view (left bottom) and partial cross-sectional (right) view of FER single crystal respectively.

Models of *k* versus *P* and *E* versus *P* used in Fig. 3A and 3B

Models for both *k* versus *P* and *E* versus *P* are available for amorphous silicas [14-19]. Bruggeman effective medium approximation (Eq. S8) has been widely used as a simple model to describe the *k versus P* relationship [15], and is plotted as the solid line in Fig. 3A.

$$f_1 \frac{k_1 - k_e}{k_1 + 2k_e} + f_2 \frac{k_2 - k_e}{k_2 + 2k_e} = 0 \qquad \text{S(8)}$$

where $f_{1,2}$, represents the fraction of the two components $k_{1,2}$, the dielectric constant of the components, and k_e, the effective dielectric constant of the material. For a porous silica binary system, k_1=4 (dense silica) and k_2=1 (air). Bruggeman's model was derived for zero frequency, but it also fits low frequency measurements such as 1 MHz, which is the most commonly used frequency for *k* measurements.

For *E* versus P, there are many predictive models for binary systems. Hashin *et al*. derived the upper and lower bounds for the effective moduli of quasi-isotropic and quasi-homogeneous materials of arbitrary phase geometry [17]. Gibon *et al*. studied the change of *E* with *P* considering both open and closed cell pores in the material [18]. A more empirical form of the relationship as shown in Eq. S9 was given by Phani *et al*. [14] and is adopted here. By fitting the data on amorphous silica given by Vella *et al*. [19], the *E* versus *P* is plotted as the solid line shown in Fig. 3B.

$$E = E_0 (1 - P)^{4.2} \qquad \text{S(9)}$$

where *E* and E_0 are the elastic moduli of porous and dense materials, respectively, and *P* is the porosity of the porous material.

The *P* of PSZ MFI, BEA, FER and CHA single crystals and polycrystalline films was calculated by comparing their FDs of them to that of quartz (e.g., FD = 26.4) as shown in Eq. S10.

$$Porosity = 100 \times (1 - \frac{FD}{26.4}) \qquad \text{S(10)}$$

The P of the spin-on films was calculated by Eq. S11, assuming the density of dense silica is 2.3 g/cm^3.

$$Porosity = \frac{Pore\ volume(cm^3/g)}{Pore\ volume(cm^3/g) + \frac{1}{2.3g/cm^3}} \qquad S(11)$$

E and k of PSZ MFI in-situ films, MFI spin-on films and MFI porogen films were from references [9, 20, 21] respectively.

References

[1] A. Gouzinis, M. Tsapatsis, *Chemistry of Materials* **1998**, *10*, 2497.
[2] Z. J. Li, S. Li, Y. S. Yan, *Advanced Functional Materials* **2004**, *14*, 1019.
[3] A. Kuperman, S. Nadimi, S. Oliver, G. A. Ozin, J. M. Garces, M. M. Olken, *Nature* **1993**, *365*, 239.
[4] F. Gao, G. Zhu, X. Li, B. Li, O. Terasaki, S. Qiu, *Journal of Physical Chemistry B* **2001**, *105*, 12704.
[5] J. J. Vlassak, W. D. Nix, *Journal of the Mechanics and Physics of Solids* **1994**, *42*, 1223.
[6] W. C. Oliver, G. M. Pharr, *Journal of Materials Research* **1992**, *7*, 1564.
[7] Z. M. Wang, R. F. Lobo, J. Lambros, *Microporous and Mesoporous Materials* **2003**, *57*, 1.
[8] J. Lin, X. F. Shu, J. X. Dong, *Materials Letters* **2005**, *59*, 1595.
[9] Z. B. Wang, H. T. Wang, A. Mitra, L. M. Huang, Y. S. Yan, *Advanced Materials* **2001**, *13*, 746.
[10] *TDR Impedance Measurements: A Foundation for Signal Integrity Application Note 55W-14601-0* **2001**.
[11] D. J. Dascher, *Hewlett-Packard Journal* **1996**, *47*, 83.
[12] S. Diamond, B. Janko, in *International Test Conference*, Baltimore, MD, **1993**, pp. 436.
[13] A. De, K. V. Rao, *Journal of Materials Science* **1988**, *23*, 661.
[14] K. K. Phani, S. K. Niyogi, *Journal of Materials Science* **1987**, *22*, 257.
[15] D. Bruggeman, *Annalen der Physik* **1935**, *24*, 636.
[16] H. Looyenga, *Physica (The Hague)* **1965**, *31*, 401.
[17] Z. Hashin, S. Shtrikman, *Journal of Applied Physics* **1962**, *33*, 3125.
[18] L. J. Gibon, M. F. Ashby, *Cellular Solids*, Pergamon Press, New York, **1988**.
[19] J. B. Vella, I. S. Adhihetty, K. Junker, A. A. Volinsky, *International Journal of Fracture* **2003**, *119*, 487.
[20] Z. B. Wang, A. P. Mitra, H. T. Wang, L. M. Huang, Y. H. Yan, *Advanced Materials* **2001**, *13*, 1463.
[21] S. Li, Z. J. Li, Y. S. Yan, *Advanced Materials* **2003**, *15*, 1528.